Operando studies of iodine species in an advanced oxidative water treatment reactor

Ahmed Moustafa,[1] Alex Evans,[1] Simmon Hofstetter,[1] Jenny Boutros,[1] Parastoo Pourrezaei,[1] Cheng Zhang,[1] Laura Patterson-Fortin,[1] Charles Laing,[1] Carter Goertzen,[1] Richard Smith,[1] Kenneth R. Code,[1] Ning Chen,[2] Peter E. R. Blanchard,[2] Nathan Bettman,[3] Raquibul Alam,[3] Kerry McPhedran,[3] Zohreh Fallah,[4] Edward P. L. Roberts,[4] and Michael W. Gaultois[5, a)]

[1)] *BioLargo Water Inc., Agrifood Discovery Place, Edmonton, AB T6H 2V8, Canada*

[2)] *Canadian Light Source, Saskatoon, SK S7N 2V3, Canada.*

[3)] *Department of Civil and Geological Engineering, University of Saskatchewan, Saskatoon, SK S7N 5A9, Canada*

[4)] *Department of Chemical and Petroleum Engineering, University of Calgary, Calgary, AB T2N 1N4, Canada*

[5)] *Leverhulme Research Centre for Functional Materials Design, The Materials Innovation Factory, Department of Chemistry, University of Liverpool, 51 Oxford Street, Liverpool, L7 3NY, United Kingdom*

(Dated: 29 July 2021)

We present an electrochemical advanced oxidation process (eAOP) reactor employing expanded graphite, potassium iodide (KI), and electrical current, which demonstrates an exceptionally high rate of inactivation of *E. coli* (10^6 or $6\log_{10}$ reduction in viable cells) at low current density (0.12 mA/cm^2), with low contact time (5 minutes) and low concentration of KI (10 ppm; 0.06 mM)). *Operando* X-ray fluorescence mapping is used to show the distribution of iodine species in the reactor, and *operando* X-ray absorption spectroscopy in the anodic chamber reveals iodine species with higher effective oxidation state than IO_4^-. *Operando* electrochemical measurements confirm the conditions in the anodic chambers are favourable for the creation of highly oxidized iodine products. The killing efficiency of this new eAOP reactor far exceeds that expected from either traditional iodine-based electrochemical water treatment or advanced oxidation systems alone, a phenomenon that may be associated with the production of highly oxidized iodine species reported here.

Keywords: wastewater treatment, advanced oxidation process, XANES, disinfection, operando electrochemistry, operando spectroscopy, iodine chemistry

I. INTRODUCTION

Advanced oxidation processes (AOPs) are emerging as a promising class of technologies for treatment of industrial and municipal waste streams for removal of recalcitrant contaminants including pharmaceuticals, pesticides, and industrial chemicals, a key facet of wastewater treatment. AOPs function by *in situ* generation of strong oxidants through a two-step process to destroy contaminants, first generating reactive oxidants and radicals that in turn react with target contaminants.[1–3] AOPs can be broadly classified as ozone- or UV-based, electrochemical, catalytic, and physical.[2,4] Full-scale processes have been established for ozone-based, UV-based, and catalytic AOPs whereas electrochemical and physical methods have been investigated exclusively at the lab- and pilot-scale.[2]

Electrochemical AOPs (eAOPs) electrolytically produce $^{\bullet}$OH and other oxidants to effect treatment of water.[1,5] The simplest eAOP is direct anodic oxidation whereby $^{\bullet}$OH is produced at the surface of an electrode through the oxidation of water.[6] Contaminants are destroyed through a combination of (1) direct oxidation of contaminants at the surface of the electrode,[7–9] (2) indirect oxidation in solution from $^{\bullet}$OH generated,[10] and (3) electric field effects.[11,12] Alternatively, indirect eAOPs require external addition of or *in situ* generation of additional reagents that react to produce hydroxyl radicals. For example, eAOPs based on Fenton's chemistry (electro-Fenton and photoelectron-Fenton) use the reaction between H_2O_2 and Fe^{2+} to produce $^{\bullet}$OH.[13,14] Oxidation may also be mediated by electrochemical generation of strong oxidants generated at the anode from ions in bulk solution[1,15] including halides like chlorine species[16–18] and iodine species.[19,20]

The inactivation of bacteria, viruses (bacteriophages), and algae using eAOPs has been demonstrated,[21–25] although the majority of past studies have focused on the electrogeneration of chlorine species.[26–29] In contrast, there is scant research on electrochemical disinfection by electrochemically generated iodine and iodine oxides, with only one bench-scale study that has examined the generation of periodate from a solution of potassium iodate.[19] eAOPs also have demonstrated effectiveness for mineralization of numerous organic compounds, and the mechanism of their action is relatively well-understood with respect to the advanced oxidation component of eAOPs. Radicals produced through advanced oxidation rapidly react with organic compounds via electron transfer, dehydrogenation, or hydroxylation

[a)] Electronic mail: m.gaultois@liverpool.ac.uk

producing organic radicals which, through the resulting radical oxidation chain, produce CO_2 and H_2O.[30,31] In contrast to advanced oxidation, the exact mechanisms of disinfection and decontamination by the electrochemical component of eAOPs are less well-understood, a problem attributed to the broad range of cellular components that can be damaged by oxidizing and reducing agents alike. Damage caused by oxidative compounds generated through electrolysis can occur to cell surfaces (cell wall, cell membrane or spore coat) and/or to cellular components (DNA, protein, lipids).[11,32] In particular, cell wall destruction is key a factor in cell inactivation by electrochemical disinfection, with significant morphological changes noted in treated cells.[33,34] However, it is important to note the mechanism of disinfection by eAOPs is likely a function of the type of anode used[11] and the identity of any halides or other electrochemically relevant compounds in the input water.

Some advantages of eAOPs include: the ability to address multiple different contaminant classes, a generally high disinfection efficiency, *in situ* production of reactive chemical species, amenability to automation, and ease of treatment input control.[15,16,31,35–37] Despite these advantages, economic and technical concerns have limited large-scale implementation of these technologies, including mass transfer limitations which lead to reduced disinfection performance, low conductance of most wastewater, limited lifespan due to fouling of the electrodes, potential accumulation of oxidation refractory intermediates, and high electricity costs.[4,31,38–42]

An Edmonton, Alberta-based water treatment technology company, BioLargo Water, has developed an electrochemical advanced oxidation process for treatment of water termed the "Advanced Oxidation System" (AOS). The AOS is a carbon-based packed-bed electrochemical water treatment system that uses expanded graphite as its electrode bed material, iodide as its principle electrochemically active input chemical, and a proprietary spacer to separate electrodes within the device. The electrode bed material chosen for the AOS reactor is expanded graphite. When intercalated graphite flakes are exposed to heat, exfoliation of the graphite occurs resulting in delamination of the graphite sheets. The resulting expanded graphite particles take on a worm-like morphology, accompanied by a dramatic increase in the surface area and number of sheet-edges and other defects often associated with electrochemical activity.[43,44] The resulting expanded graphite is a carbon-based material with high surface area, high porosity, and high electrical conductivity,[45,46] and these qualities are ideal for packed bed electrochemical reactors. Expanded graphite is also inexpensive and widely available, and thus presents an economically feasible solution for decentralized water and wastewater disinfection.

While the reactor geometry is flexible, the device typically has 6 serial chambers (3 cathodes and 3 anodes), and is designed this way to provide multiple instances of bactericidal action for water passing through it (Figure S1a). This AOS design has been shown to be scalable for field demonstration pilots that process 20 litres per minute (at a poultry wastewater treatment pilot in Alberta)[47] and 400 litres per minute (at a municipal wastewater treatment pilot near Montreal).[48] The AOS reactors described and used in the present work were designed to enable the electrochemical and XANES analyses, but are similar in design to scaled-up versions of the reactor.

The AOS uses potassium iodide as its input chemical to drive disinfecting oxidation reactions at the anodic chamber. Iodine is a strong oxidant and long-studied disinfectant; when exposed to bacteria, iodine interferes with bacterial cellular function by oxidizing or iodinating proteins, nucleotides of DNA or RNA, or fatty acids, ultimately leading to cell death.[19,49–51] While molecular iodine (I_2) is generally thought to be the principle species of iodine responsible for bacterial inactivation, hypoiodous acid (HOI) and periodate ($[IO_4]^-$) are also known to exhibit bactericidal properties.[19,49,50]

In this study we present an electrochemical reactor capable of disinfection with high kill efficiency, short contact times, low current, and low concentrations of active species. Using the BioLargo AOS, we demonstrate 1) disinfection in a carbon-based packed-bed electrochemical water treatment system, and 2) novel electrochemical species generated by this specific proprietary water treatment device (the AOS). The killing efficiency of this new electrochemical reactor exceeds that expected from either iodine-based electrochemical disinfection or from other advanced oxidation processes. The mechanism of this synergistic activity is hypothesized to be associated with the production of highly oxidized iodine species observed in this study.

II. METHODS

A. Microbiological studies

Escherichia coli MC4100, a variant of *E. coli* K12, was used in this study. *E. coli* was chosen for these studies due to its relevance in wastewater treatment and its conduciveness for future mechanistic studies on the AOS. Specifically, the availability of open reading frame mutant libraries for *E. coli* K12 facilitates mutational analyses, and the stress responses of are exceptionally well characterized. Furthermore, most electrodisinfection studies published in the last decade used *E. coli* as a model organism, making it the most suitable candidate in the context of the existing body of research in this area.[27] Bacterial cultures were grown in Luria-Bertani (LB) medium at 37 °C and aerated by shaking at 150 rpm. Overnight cultures were harvested and resuspended in 5 L reverse osmosis (RO) water. Potassium iodide (KI; 10 ppm, 10 mg/L, 0.06 mM) was added where indicated.

Inactivation of *E. coli* using the AOS technology was

performed using a 2" diameter 6-chamber reactor packed as described above. RO water seeded with $\sim 10^8$ CFU/mL *E. coli* was passed through the AOS reactor at 80 mL/min under the following conditions: 0 V, 0 ppm KI; 6 V, 0 ppm KI; and 6 V, 10 ppm KI. Samples were collected at 10 minute intervals for a total of 60 minutes. The number of viable *E. coli* cells after treatment was determined by spiral plating 50 μL aliquots on LB agar. To clean the reactor prior to each experiment, the reactor was flushed with 30 ppm KI at 80 mL/min under 6 V electrical potential for 30 minutes; mixing is achieved through flow passing through the randomly packed bed reactor. The electrical polarity was then inverted for 15 minutes without flow, after which time the reactor was then flushed with RO water for 30 minutes at 80 mL/min. This flushing protocol was also repeated after each experiment.

To identify where disinfection occurs, RO water seeded with $\sim 10^8$ CFU/mL *E. coli* was passed through a horizontal 1" diameter, 2-chamber reactor at 20 mL/min, with 50 ppm KI at 12 V for 60 minutes (Figure S1b). The higher concentration of KI and higher voltage is required owing to obtain similar levels of bacterial inactivation in this alternate reactor configuration. The horizontal orientation and split flow to the anodic and cathodic chambers allow bacteria to pass through either the anodic or cathodic chamber, but not both. Samples were collected at 15 minute intervals for a total of 60 minutes. The number of viable *E. coli* cells after passage through the anodic or cathodic chambers were determined by spiral plating 50 μL aliquots on LB agar. Prior to each experiment, the reactor was flushed with RO water for 30 minutes at 20 mL/min. After each experiment, the reactor was cleaned by flushing with 50 ppm KI solution for 120 minutes at 20 mL/min under 12 V applied potential, with a reversed bias after 60 minutes.

B. Operando I K edge X-ray spectroscopy

Measurements were performed at the HXMA beamline at the Canadian Light Source.[52] The beamline energy for the I K-edge at 33169 eV was calibrated to the Sb K-edge at 30491 eV using Sb foil collected in transmission geometry; ion chambers were filled with 5% Ar and 95% N_2. All data of solutions presented in this work was collected in fluorescence geometry using the 32-element Ge detector, as absorption through the diameter of the reactor leads to a weak transmission signal. *Operando* measurements of the reactor were performed in 3 different conditions: pristine (0 mL/min 1000 ppm KI, 0 V), flow mode (4 mL/min 1000 ppm KI, 12 V), and batch mode (0 mL/min 1000 ppm KI, 12 V).

A motorized stage was used to control the position of the reactor with respect to the X-ray beam. X-ray fluorescence (XRF) maps were collected using an X-ray beam of dimensions 2 mm $\times$ 1 mm (width $\times$ height); the reactor was mapped with a 2 mm $\times$ 2 mm spatial grid, with a 2 second dwell time per grid point.

X-ray absorption near edge structure (XANES) measurements were collected using an X-ray beam of dimensions 3 mm $\times$ 1 mm. A wider beam was used to improve the signal and decrease the influence of any inhomogeneity in the reactor. Data was collected from -100 eV to -40 eV at 5 eV steps, -40 eV to 50 eV at 1 eV steps, and 50 eV to $7k$ at $0.1k$ steps, with dwell times of 2 seconds in each region, resulting in a scan time of $\sim$10 minutes. At least 2 scans were collected for each measurement to ensure reproducibility. Data was analyzed using the ATHENA software package.[53]

1000 ppm (1 g/L) standard solutions of reference compounds were prepared by dissolving solid powders in appropriate amounts of deionized water (18.2 MΩ cm), or hexanes for I_2. Solid reference samples were prepared by finely grinding a compound of interest in an agate mortar and pestle, then diluted by grinding together with boron nitride, and packed to create a solid with appropriate absorption at the I K edge. XANES data collection of solids was performed in transmission geometry, and spectral features are consistent with fluorescence spectra of the corresponding 1000 ppm solutions made by dissolving the solids in water.

Iodine species are known to transform, so to ensure there was no unintentional evolution of iodine species over time, standards were examined again 24 hours after initial preparation and data collection; no differences were seen in any X-ray spectral features, indicating the species examined here undergo no significant transformation without intentional perturbation over the experimental timelines in this study.

C. Ex situ cyclic voltammetry

To determine the electrochemical characteristics of the expanded graphite used in the AOS reactor, cyclic voltammetry (CV) experiments were performed. Pellet electrodes were prepared by compressing samples of expanded graphite using a compression molder. The prepared pellets, with a fixed density, were used as the working electrode. A platinum wire was used as the counter electrode and a silver/silver chloride (Ag/AgCl in saturated KCl) was used as a reference electrode. An Autolab PGSTAT 302N potentiostat was used to carry out the cyclic voltammetry experiments with a potential window of 0.0 V to 1.0 V and a scan rate of 0.01 V s^{-1}. The background electrolytes used used in all CV measurements were 0.1 M phosphate buffer (pH 7.6) and 0.1 M Na_2SO_4). Potassium iodide solutions were prepared using deionized water, with 100 ppm KI (0.6 mM) in addition to the background electrolyte.

D. Operando potential distribution measurement

A cylindrical AOS reactor with two anodes and one cathode was designed for potential distribution studies

(Figure S1c). Local potentials were determined during reactor operation by measuring the potential difference between the expanded graphite bed and the solution passing through it at different positions (height) in the reactor. Ag/AgCl reference electrodes were located in an external container connected to the bed via capillary tubes, and the bed solution was released to the container using the water outlets for each measurement. At each position (height), the local potential difference was measured between the graphite rod and the capillary connected to the reference electrode. An Autolab PGSTAT 302N potentiostat was used to apply a constant voltage between the expanded graphite electrodes and to monitor the current during the process.

Graphite rods at position 1 and 9 were used as the anode current feeders connected to the potentiostat, and the rod at position 5 was used as the cathode current feeder. The local potential of the expanded graphite relative to the Ag/AgCl reference electrode at different locations in the expanded graphite electrodes (position 7, 8 and 9) and the cathode (position 4, 5 and 6) was measured during operation using a high impedance digital voltmeter, while a cell potential of 10 V was applied between the anodes and the cathode. Potential measurements in the AOS reactor were carried out with a solution feed composition of 0.6 mM KI and 28 mM Na_2SO_4 (100 ppm KI and 4000 ppm Na_2SO_4). Using a cell voltage of 10 V, the total current was 9.42 ± 0.01 mA. The flow rate of the solution was fixed at 100 mL/min using a peristaltic pump.

E. Preparation of expanded graphite electrodes

Intumescent graphite (grade 3772; Asbury Carbons) was used to prepare the expanded graphite electrodes following a previously reported protocol.[54] Flakes were heated in an oven at 1000°C for 75 seconds and then taken out from the oven and allowed to cool at room temperature. This expanded graphite was then weighed and mixed with distilled water to create a slurry, which was added to the empty reactors and packed to form the final packed bed reactors. The 2" diameter, 6-chamber reactor used in the present work contains $\sim$1.45 g graphite in each electrode. The Brunauer–Emmett–Teller (BET) surface area of expanded graphite prepared in this manner has been measured to be $77 \pm 1\,m^2/g$,[54] so the total surface area of the expanded graphite in the 6-chamber reactor is estimated to be 112 m^2 per electrode (335 m^2 for the 3 anodes connected in parallel). The current density reported in the present work is calculated using only the projected anodic surface area, taken from the inner diameter of the reactor across 5 active anodic surfaces in the reactor (0.12 mA/cm^2; $I/(5\times\pi r^2)$, where $I = 12$ mA and $r = 2.5$ cm).

III. RESULTS AND DISCUSSION

A. Rapid disinfection of model bacteria

To study the means of disinfection that occurs in the AOS reactor, a series of experiments were designed to evaluate the influence of: potassium iodide, electrical potential, and expanded graphite on bacterial disinfection performance. The AOS operated at 6 V and/or 10 ppm input KI. The iodide (I^-) concentrations used in the AOS system do not exceed the United States Environmental Protection Agency maximum tolerance level of 25 ppm titratable iodine.[55] Further, 10 ppm KI (10 mg/L; 0.06 mM) used in standard operation of the AOS is a concentration that is within acceptable water treatment discharge limits for potassium iodide in Alberta and most jurisdictions in Canada. Further, 10 ppm KI is the same concentration used with the AOS in a recent study that demonstrated no adverse biological effects in two model aquatic organisms.[56]

AOS disinfection experiments were performed for 1 hour using RO water seeded with $\sim 10^8$ CFU/mL *E. coli*. The number of *E. coli* in the influent and effluent were quantified using total plate counts on LB agar. At the beginning of each experiment, similar levels of *E. coli* were detected in the influent. In the presence of 10 ppm KI and 6 V, *E. coli* counts decreased below the quantification limit (LoQ = 4×10^2 or $2.6\log_{10}$) within 10 minutes, representing a 10^6 or $6\log_{10}$ reduction (Figure 1a). In contrast, in the absence of KI but the presence of 6 V, no significant decrease in *E. coli* numbers in the treated effluent was observed (Figure 1b). Similarly, in the absence of both KI and power, no significant decrease in bacteria was observed (Figure 1c). Taken together, these results indicate that both potassium iodide and electrical potential are required for inactivation of bacteria in water using the AOS technology.

The physical integrity of Gram negative bacterial cells treated using the AOS was studied using transmission electron microscopy (TEM)[57] and live/dead staining and fluorescent microscopy (Figure S2).[58] TEM reveals structural changes to the cells suggesting decreased membrane integrity, but no evidence of cell lysis was observed. Accordingly, live/dead staining and fluorescent microscopy was performed, which confirmed the cells were dead but physically intact. This is consistent with previous studies on electrochemical disinfection systems that observed morphological changes to cell wall structure, where destruction of the cell wall was a key factor for cell inactivation.[5,33,34]

Iodine oxidants electrochemically generated within the AOS are thought to be the molecules principally responsible for disinfection within the device. In keeping with this theory, the minimal rates of bacterial inactivation observed in the absence of potassium iodide but in the presence of electrical potential suggests the observed decrease in *E. coli* counts cannot be attributed to electrochemically generated hydroxyl radicals and/or

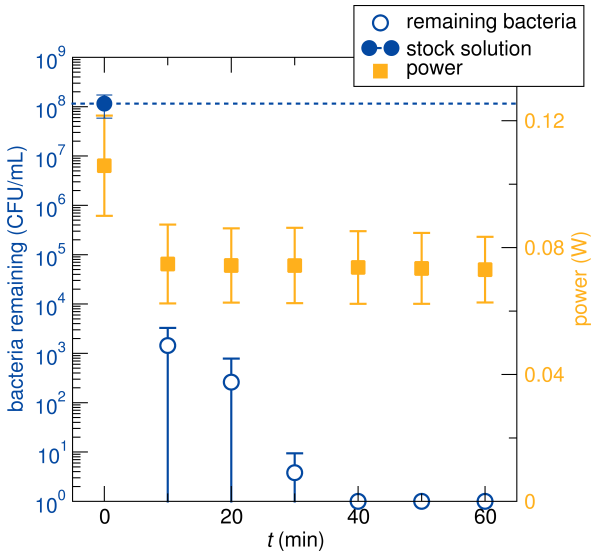

(a) 6 V, 10 ppm KI

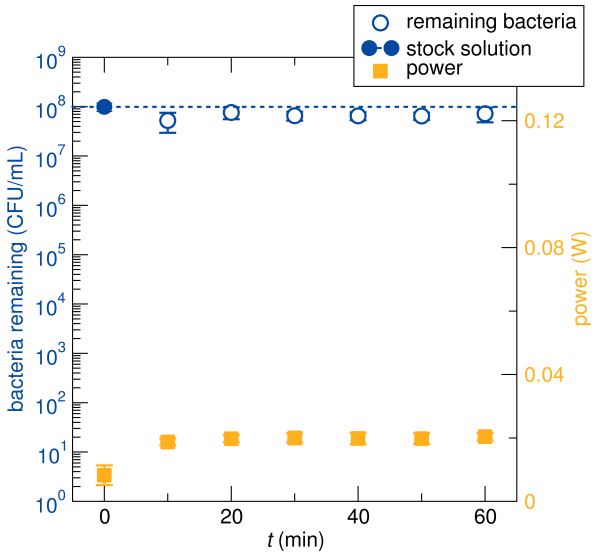

(b) 6 V, 0 ppm KI

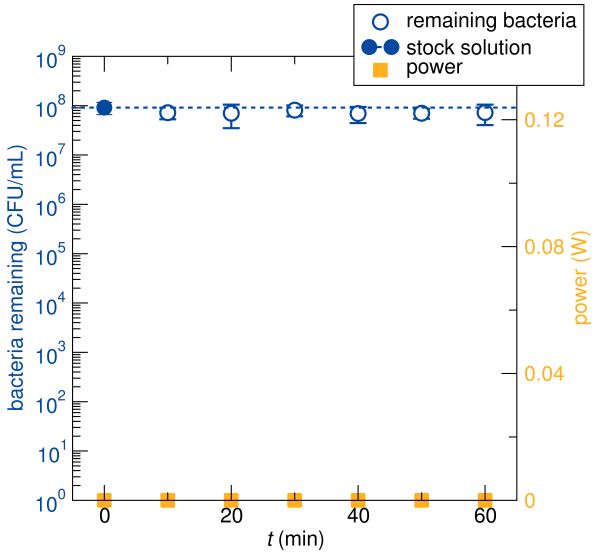

(c) 0 V, 0 ppm KI

FIG. 1: RO water seeded with $\sim 10^8$ CFU/mL *E. coli* was passed through a 2", 6-chamber AOS reactor at 80 mL/min. (a) 6 V, 10 ppm KI; (b) 6 V, 0 ppm KI; (c) 0 V, 0 ppm KI. Stock *E. coli* in CFU/mL (circles), CFU/mL $\sim 10^8$ CFU/mL *E. coli* remaining after treatment (squares), and power consumption of the reactor (triangles). Results are expressed as the mean; error bars represent the standard deviation from triplicate experiments. The AOS reactor is effective at inactivating *E. coli* only in the presence of all three components: expanded graphite, KI in solution, and an applied electric potential.

direct oxidation at the anode surface. Similar results have been found for electrochemical disinfection using a range of electrodes including boron-doped diamond (BDD) and tin-tungsten-oxide where bacterial inactivation was shown to be attributed to reactive chlorine species with negligible contribution from $^{\bullet}$OH or other reactive oxygen species at current densities similar to those examined in our study.[11,25,27,28] The contribution of adsorption to the electrode surfaces was also minimal in the AOS reactor, as demonstrated by the absence of significant bacterial inactivation in the absence of iodine and/or electrical potential. The absence of attachment or adsorption to electrode surface has also been shown for electrochemical cells with mixed metal anodes.[11]

To determine which electrochemical chamber, anodic or cathodic, is responsible for the bacterial inactivation exhibited by the AOS, an experiment was designed whereby a horizontally oriented AOS reactor was run continuously for 1 hour with outgoing ports on each chamber. RO water seeded with $\sim 10^8$ CFU/mL *E. coli* was passed through the reactor. Within 15 minutes, *E. coli* counts decreased below the quantification limit, approximately a 10^6 or $6\log_{10}$ reduction (Figure 2). No bacteria were detected in the effluent collected from the anodic chamber. This is in contrast with the effluent collected from the cathodic chamber where the viable bacterial concentration was equal to that of the influent feed water and did not change over the course of the experiment (Figure 2). These results indicate that inactivation of bacteria in the presence of potassium iodide and electrical potential occurs within the anodic chamber. Anodic generation of disinfecting species, predominately reactive chlorine species, has been shown in electrochemical cells composed of BDD, graphite felt/PbO_2, antimony-doped tin-tungsten-oxide, and BiO_x/TiO_2 electrodes.[11,25,28,59] Furthermore, periodate ($[IO_4]^-$) electrochemically generated from a potassium iodate solution has been shown to inactivate *E. coli*,[19] though this is the only previous report of electrochemical generation of iodine species for disinfection.

The hydraulic retention time and current density (based on the projected area of the electrode) required to achieve a $6\log_{10}$ reduction using the AOS technology

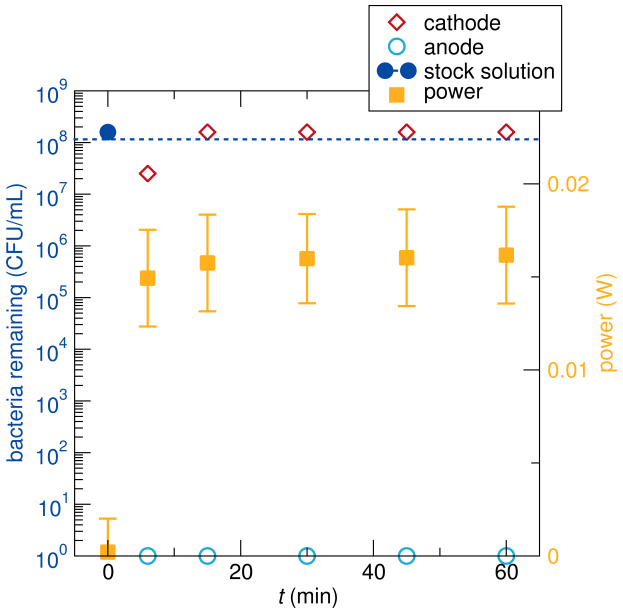

FIG. 2: RO water seeded with ∼10^8 CFU/mL *E. coli* was passed through a horizontal 1" diameter, 2-chamber AOS reactor at 20 mL/min, 50 ppm KI, and 12 V. Stock *E. coli* in CFU/mL (filled circles), CFU/mL *E. coli* remaining cathodic chamber (hollow diamond), CFU/mL *E. coli* remaining anodic chamber (hollow circle), and power consumption of the reactor (square). Measurements from the aliquots taken from the cathodic chamber show no decrease in *E. coli* counts, whereas measurements from aliquots taken from the anodic chamber demonstrate inactivation of *E. coli*.

was 5 minutes and 0.12 mA/cm^2. This is discussed in the context of relevant studies (Table I), which are taken from a recent critical review of electrochemical disinfection of bacteria.[27] The retention time in the AOS is similar to published values for *E. coli* inactivation from other studies using electrochemical cells. In general, as current density increases, reaction time decreases until a threshold value for current density is reached.[9,11,60] Ghasemian *et al.* showed that a cell composed of a mixed metal-oxide electrode required 5 minutes for a inactivation of a 7.4log$_{10}$ *E. coli* solution at a current density of 2 mA/cm^2; the system threshold was reached at 6 mA/cm^2, where inactivation was achieved in 1 minute. Similarly, for a BDD system, a 4log$_{10}$ reduction in *E. coli*, *Pseudomonas aeruginosa*, *Pseudomonas fluorescens*, and *Bacillus subtilis* spores was reported in contaminated tap water within 5.5 mins at 2 mA/cm^2, and the time to achieve a threshold disinfection of 4log$_{10}$ decreased as current density increased.[61] Another report using a BDD-based system reported the time to achieve a threshold disinfection of 4log$_{10}$ decreased as the current density increased from 7.5 mA/cm^2 to 120 mA/cm^2.[28] Operating on municipal wastewater effluent, a BDD-based eAOP was employed as a simulated pre-chlorination tertiary treatment step for a contaminated wastewater stream,

TABLE I: Comparison of reported electrochemical advanced oxidation processes (eAOPs) with similar hydraulic retention times and model organisms. All studies presented here report successful inactivation. A more detailed version is available in the supporting information (Table S1).

Report	Stock solution (log CFU/mL)	Retention time (min)	Current density (mA/cm^{-2})	Energy consumption (kWh m^{-3})
This work	8	5.0	0.12	0.016
Ref. [11]	7.4	5.0	2.0	0.064
Ref. [28]	6	1.4	7.5	0.045
Ref. [61]	4	5.5	2.0	0.104
Ref. [29]	4	n/a	7.5	<0.2
Ref. [62]	3	1.5	2.1	0.2
Ref. [60]	7.4	10.0	208	0.75

and demonstrated successful disinfection of *E.coli* after 1.5 minutes at a current density of 2.1 mA/cm^2.[62]

In the context of other work, the AOS used in the present work required an order of magnitude lower current density at a comparable retention time to achieve similar bacterial kill kinetics (Table I). This could be a result of factors including: A) greater titers of active iodine oxidants generated within the AOS anodic chamber compared to other electrochemical systems, and/or B) the generation of more active iodine oxidants that increase the disinfection potential of the AOS compared to similar electrochemical systems. *Operando* X-ray absorption studies described below reveal the presence of highly oxidized iodine species, which is consistent with the latter hypothesis. Importantly, the performance of the AOS leads markedly lower energy consumption (0.0156 kWh m^{-3}) than comparable technologies (Table I), and although a full cost analysis is not considered here given the small scale of the reactor used in this work, the low operational (and material) costs of the AOS would make this technology favourable for use in treatment facilities where operation and maintenance costs need to be minimized.

B. Operando mapping of iodine distribution using I K edge X-ray fluorescence

To determine the location of the iodine species believed to be responsible for the exceptional killing efficiency observed in the biological studies shown above, X-ray fluorescence (XRF) mapping at the iodine K edge (∼33 keV) was performed on a 6-chamber BioLargo AOS reactor during operation (Figure 3). The fluorescence intensity is proportional to the number of iodine atoms being irradiated, and the high energy X-rays characteristic of the I K edge penetrate the reactor and allow a true bulk measurement of the spatial distribution of iodine species present – the absorption length, or the distance

after which the irradiating beam intensity has decreased to $1/e\, I_0 \approx 0.37\, I_0$, at 33 keV in water is $\lambda = 3$ cm.

XRF mapping using a motorized stage was performed to determine the spatial distribution of iodine within the reactor during operation. (Absorption spectra were collected subsequently at regions of interest during each operation mode to determine the nature of the iodine species present, described later.) A 6-chamber BioLargo AOS reactor filled with 1000 ppm KI was mapped using XRF while in 3 different conditions: pristine (0 mL/min 1000 ppm KI, 0 V), flow mode (4 mL/min 1000 ppm KI, 12 V), and batch mode (0 mL/min 1000 ppm KI, 12 V).

The 6-chamber reactor used for the synchrotron experiments is 14.5 cm high and 3.0 cm inner diameter, and when fully packed, has a void fraction of 51% and thus a column volume corresponds to ∼50 mL. To flush the reactor after operation, 30 equivalent column volumes of deionized water are flushed through the reactor at a rate of 1 column volume per minute. A separate experiment using the same flow rate, and a similarly packed reactor filled with a solution containing strongly coloured organic dye, determined that flushing with 30 column volumes of deionized water leads to a 10^3 reduction in dye concentration. The organic dye has similar affinity to the expanded graphite as iodine, so flushing with a large excess of deionized water ensures any remaining species in solution initially in the reactor are nearly removed (*i.e.*, are diluted by a factor of 1000).

In the pristine reactor filled with an aqueous solution of 1000 ppm KI (0 mL/min 1000 ppm KI, 0 V applied across the reactor), XRF maps show uniform intensity, indicating I is evenly distributed throughout the reactor (Figure 3b). The reactor was then operated in flow mode with the same solution (4 mL/min 1000 ppm KI, 12 V), and XRF maps reveal increased relative and absolute fluorescence intensity at the anodic regions (Figure 3c). In addition to indicating I is heterogeneously distributed in the reactor during operating conditions, the significantly higher *absolute* intensity suggests I preferentially accumulates in the anodic chambers. Following the flow studies, the reactor was flushed with excess deionized water to remove any excess I species.

Finally, the reactor was flushed with 1000 ppm KI solution and then operated without flow in batch mode (0 mL/min 1000 ppm KI, 12 V), and the corresponding XRF map displays higher relative intensity at anodic regions despite having no flow (Figure 3d). This heterogeneity does not become expressed until an electric potential is applied across the reactor, suggesting enrichment of the anodic regions is likely aided by electromigration. Activated carbon materials are known to physically adsorb iodine, though given the reactor conditions it is likely that electrochemical reaction and subsequent modification of the expanded graphite and/or chemical incorporation and absorption of iodine species may occur to some extent. Nevertheless, the potential presence of these species alone does not lead to inactivation of *E. coli* if water is subsequently passed through the reactor; the presence of all components mentioned earlier is still necessary: expanded graphite, KI, and an applied electric potential.

C. Operando speciation of iodine using I K edge X-ray absorption spectroscopy

To determine the nature of the active species responsible for the exceptional killing efficiency observed in the biological studies shown earlier, iodine speciation using X-ray absorption spectroscopy (XAS) was performed on all chambers during operation of the reactor. As described earlier, the high energy of the incident X-rays at the I K edge are highly penetrating, and provide a bulk measurement of the iodine species present in the reactor.

Importantly, we distinguish here the oxidation state, which we treat to be directly related to the ground state charge density and the degree of electron deficiency, from the formal charge, which is the charge assigned to an atom under the assumption of complete charge transfer in a compound with purely ionic interactions. Iodine is large and polarizable, and the strong bonding within polyoxo anionic species discussed here lead to bonding very far from this ionic limit. Formal charges are thus used here to compare the relative oxidation state. For example, *e.g.*, iodine in $[IO_3]^-$ is formally I^{5+}, whereas iodine in $[IO_4]^-$ is formally I^{7+}. This merely implies iodine in $[IO_4]^-$ is more electron deficient than $[IO_3]^-$, and not that iodine in $[IO_4]^-$ has no electrons.

The I K edge X-ray absorption near edge structure (XANES) is characteristic of the iodine oxidation state, which allows the determination of the iodine species in the reactor.[63–65] Specifically, as the oxidation state of iodine increases – the ground state electron density at iodine decreases and iodine becomes more electron deficient – the onset energy and the intensity of the primary absorption feature increase. With increasing oxidation state, the remaining electrons on iodine are lower in energy and thus more difficult to promote to unoccupied states, increasing the observed X-ray absorption energy observed. Similarly, with increasing oxidation state there are more unoccupied iodine electronic states, which increases the transition probability and thus the intensity of the X-ray absorption feature.

When there are multiple species present, the resulting spectrum is a linear combination of the two component spectra, which allows semi-quantitative determination of iodine species present. Although the relative concentration of species with respect to each other can be determined, to aid identification, the lineshape and peak intensity in the spectra reported here are normalized to a single absorbing atom and are thus independent of the absolute concentration – lower absolute concentration will merely lead to spectra with more noise.

Solid powder and 1000 ppm solution standards of reference compounds were prepared to facilitate identification of iodine species and relative oxidation states (Fig-

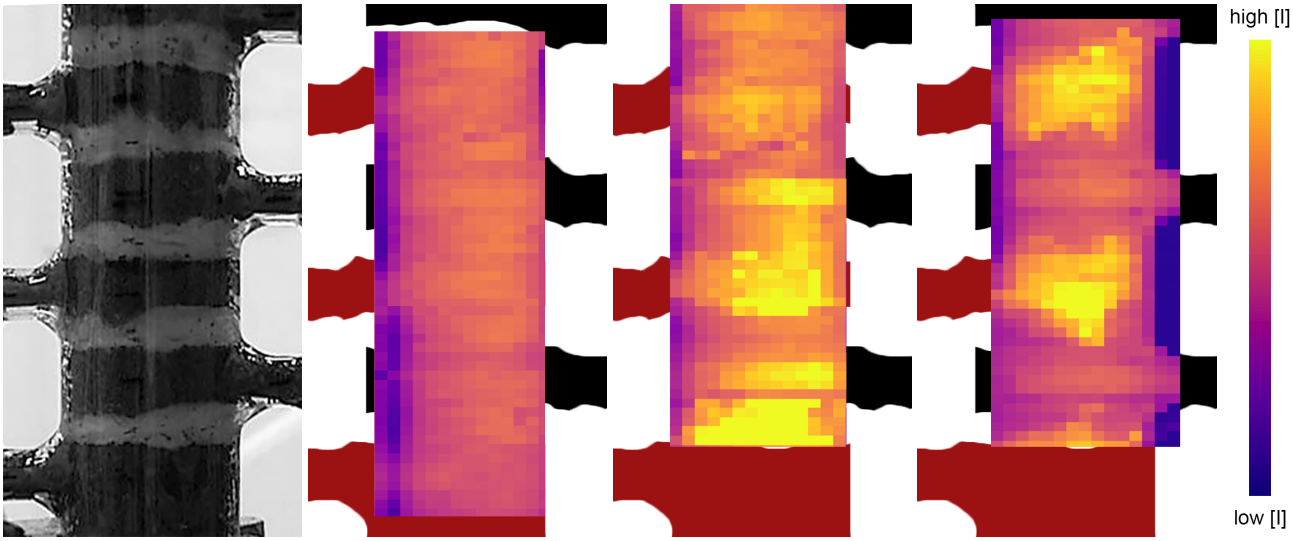

(a) (b) (c) (d)

FIG. 3: (a) Photo of the 6-chamber reactor, as mounted at the beamline, where anodic chambers (red in simplified representation) are connected at the left of the apparatus, cathodic chambers (black in simplified representation) are connected at the right. (b-d) X-ray fluorescence (XRF) maps of total I species overlaid on the simplified representation of the 6-chamber reactor. Yellow corresponds to regions of high I concentration (see colour bar). (b) An XRF map of I species in a pristine reactor demonstrates I is homogeneous before operation. (c) An XRF map of the reactor operating in flow mode (4 mL/min 1000 ppm KI, 12 V) exhibits increased absolute and relative fluorescence intensity at anodic regions, indicating I preferentially accumulates in anodic chambers. (d) An XRF map of the reactor operating in batch mode (0 mL/min 1000 ppm KI, 12 V) displays higher relative intensity at anodic regions despite having no flow, suggesting electromigration likely takes place to enrich I concentration in anodic chambers.

ure S3); reference spectra shown here are consistent with previous reports.[63–65] Solution species show similar spectral features (*e.g.*, the absorption energy and peak intensity) to solid compounds with the same formal charge, as the absorption energy and peak intensity depend primarily on the oxidation state of iodine. Notably, the spectral features of the solution species are slightly broader in energy than their solid analogues, as the chemical environment around iodine is not as uniform in solution as in a crystalline powder, leading to a larger distribution of states in energy.

Oxidized iodine species are clearly distinct from iodine species with lower oxidation state. As described earlier, the increasing iodine oxidation state leads to an increased absorption energy, and, most notably and diagnostically, a large peak intensity at the absorption edge due to an increased probability of transition to a larger number of unoccupied electronic states. This peak intensity increases with oxidation state, as can be seen in the evolution from I^{5+} species to I^{7+} species (Figure S3).

XANES measurements performed on anodic chambers of the operating reactor consistently produce spectra with increased absorption energy and peak intensity compared to $[IO_4]^-$ (Figure 4), which has the highest formal charge of reference species measured here. Although the identity of the species cannot be determined, the increased absorption energy and peak intensity unambiguously indicate this new species being formed in the reactor has iodine which more electron deficient than $[IO_4]^-$.

We suggest the *in situ* generation of this highly oxidized species may be responsible for the exceptional killing efficiency observed in the biological studies reported above. As discussed in the experiments reported in following sections, this killing efficiency can not be attributed to other possible biological stressors generated by the reactor, such as changes in pH, electrical potential, and/or hydroxyl radicals. These processes are known to occur in any electrochemical oxidative water treatment processes, though the exceptional killing activity observed here is only observed in the presence of iodine species.

In contrast to the anodic chambers, X-ray absorption spectra collected from the cathodic chambers are consistent with I^- (Figure S4), suggesting any active species generated in the anodic chamber are reduced in the subsequent cathodic chamber. XANES measurements performed on the cathodic chambers have much lower signal intensity than anodic chambers due to the preferential accumulation of I species in the anodic chambers observed by XRF mapping discussed earlier; the spectrum from the cathode shown in Figure S4 required a factor of 4 increase in collection time, but nevertheless there is no evidence for the presence of highly oxidized species

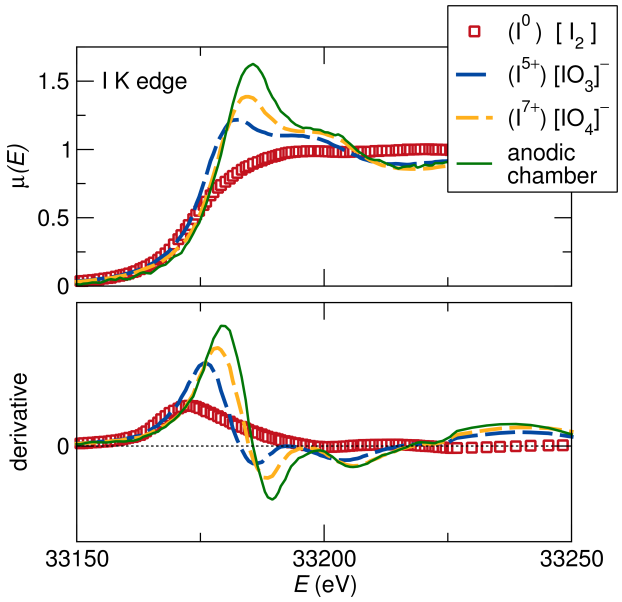

FIG. 4: Compared to iodine in lower oxidation states (*e.g.*, I_2), the XANES of iodine in higher oxidation states has a higher absorption energy, and a pronounced peak whose intensity increases with oxidation state. I K edge XANES of the anodic chambers in the reactor has a higher absorption energy and peak intensity than any reference compound measured here or seen in the literature, suggesting the presence of an iodine species more oxidized than $[IO_4]^-$.

in the cathodic chambers, nor do we see evidence of any species other than I^-.

Measurements of the glass wool spacers did not have sufficient signal to determine the presence of any iodine species. Moreover, spectra collected from the effluent are consistent with spectra consistent with I^- (Figure S4), suggesting that to within the limits of the technique, any species generated are no longer present in the reactor effluent.

D. Ex situ cyclic voltammetry of iodine species at an expanded graphite electrode

Operando XANES measurements of the AOS reactor reveal the presence of a highly oxidized iodine species when the reactor is operated in the presence of a 1000 ppm KI solution. 1000 ppm KI was chosen because it is the lowest concentration at which sufficient signal can be obtained from XANES measurements with relevant data collection times, while still remaining in a possible operational window of the reactor. Nevertheless, the exceptional killing efficiency of the AOS reactor can be demonstrated at concentrations as low as 5 ppm KI,[66] and anticipated treatment applications are expected to operate at concentrations <25 ppm KI. Accordingly, *ex situ* and *operando* electrochemical methods were performed to investigate the redox species being generated at lower iodine concentrations.

In order to determine the electrode potentials required to drive the desired reactions inside an AOS reactor, and in order to characterize the electrochemical properties of the expanded graphite used in AOS reactors, cyclic voltammetry (CV) was carried out. A voltammogram was recorded using a background solution in the absence of iodide; no redox reactions were observed at pH 7.6 within a potential window of 0.0 V to 1.0 V versus Ag/AgCl (Figure S5). However, in the presence of iodide, three redox couples are observed at half-cell potentials of $E_{1/2} = 0.37$ V, 0.51 V and 0.68 V, as well as an anodic peak near 0.9 V versus the Ag/AgCl reference electrode. Based on the standard reduction potentials of iodide oxidation reactions (Equations (1) to (3)),[67–71] the redox couples at 0.37 V and 0.51 V are attributed to a two-step redox reaction shown in Equation (1) and Equation (2). The first peak at 0.37 V shows the oxidation of I^- to I_3^- and the second peak at 0.51 V shows the oxidation of I_3^- to I_2.[72,73] (It is possible the two peaks may be associated with a combination of adsorption and electron transfer steps.[68,69,73] However, coupled electrochemical reactions and adsorption processes can complicate the voltammetry, and more detailed studies beyond the scope of this work would be needed to confirm the reaction mechanism.) The redox couple observed at 0.68 V versus Ag/AgCl is attributed to the I^-/IO_3^- redox process (Equation (3)). Accounting for the effect of the pH, the redox potential of this reaction is expected to be around 0.68 V versus Ag/AgCl at a pH of 7.6. The anodic peak observed at 0.9 V versus Ag/AgCl is attributed to oxidation of iodate to periodate (Equation (4)) accounting for the effect of pH on the redox potential.[19,74,75]

$$3\,I^- \rightleftharpoons I_3^- + 2\,e^- \tag{1}$$

$$2\,I_3^- \rightleftharpoons 3\,I_2 + 2\,e^- \tag{2}$$

$$I^- + 3\,H_2O \rightleftharpoons IO_3^- + 6\,H^+ + 6\,e^- \tag{3}$$

$$IO_3^- + 2\,OH^- \rightleftharpoons IO_4^- + H_2O + 2\,e^- \tag{4}$$

E. Operando potential distribution measurement of an AOS reactor

The electrode potential, corresponding to the potential difference between the expanded graphite electrode and the solution, determines the electrochemical reactions occurring in the AOS reactor. Accordingly, a reactor was modified to measure the distribution of the electrical potential within the electrode chambers (Figure S1c), with the goal of probing the electrochemical reactions occurring at the electrodes during operation of the reactor.

The measured local potential in the electrode bed at different positions relative to the glass wool spacer in the AOS reactor is shown in Figure 5. In order to oxidize I^- to IO_3^-, potentials more positive than 0.68 V ver-

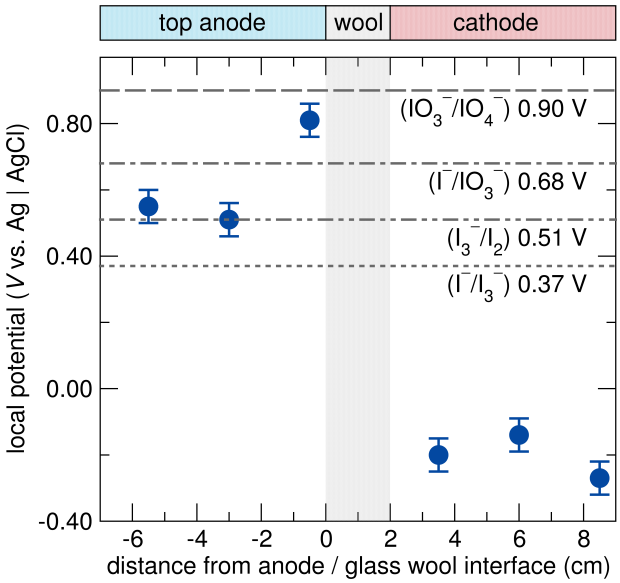

FIG. 5: Distribution of electrical potential in the anode and cathode chambers of the AOS reactor during current and solution flow. The applied cell voltage was 10 V, and the current was 9.42 mA. The solution flow rate was 100 mL/min, with a composition of 100 ppm KI and 4000 ppm Na_2SO_4 (0.6 mM KI, 28 mM Na_2SO_4). The long dashed line corresponds to the 0.9 V potential required for redox reaction of IO_3^- to IO_4^- at pH 7.6 (as determined by the cyclic voltammetry). The dot-dashed line corresponds to the 0.68 V potential required for redox reaction of I^- to IO_3^- at pH 7.6, and the remaining dotted lines correspond to the I^-/I_3^- and I_3^-/I_2 redox reactions occurring at 0.37 V and 0.51 V.

sus Ag/AgCl are required at pH 7.6, while IO_3^- can be reduced to I^- at potentials less positive than 0.68 V. Similarly, at potentials above 0.5 V I^- can be oxidized to I_2 and below 0.37 V reduction to I^- will occur. At potentials above 0.9 V, IO_3^- can be oxidized to IO_4^- at pH 7.6.

In the cathode of the AOS reactor (position 4, 5 and 6), all local electrode potentials were less than the redox potential for the I^-/I_3^-, I_3^-/I_2 and I^-/IO_3^- couples and also for the IO_4^-/IO_3^- redox processes, which indicates that at all positions in the cathode of the AOS it is expected that iodine in higher oxidation states will be reduced to iodide. In the anode, the electrode potentials at position 8 and 9 are not sufficient for iodate formation, but are just sufficient for iodine and triiodide formation. At position 7, close to surface of the anode facing the cathode, the electrode potential was measured to be 0.81 V versus Ag/AgCl, which is sufficient for formation of iodine, triiodide and also iodate at pH 7.6. However, the electrode potential increases rapidly towards the surface (where the anode meets the glass wool), due to ohmic losses in the solution as the current flows into the porous electrode. At this interface between the anode and the glass wool, the electrode potential should be significantly higher than 0.81 V,[76] leading to formation of periodate or species with higher oxidation states along with iodate, iodine and triiodide.

Further, The pH of the solution in the top glass wool between the to the cathode and the top anode electrode was found to be pH∼11.5. This high pH decreases the redox potential for I^-/IO_3^- and IO_4^-/IO_3^- redox processes, facilitating the formation of the iodate and periodate at the anode. Similarly, acidic conditions in solution flowing in the bottom glass wool entering the cathode (where the pH was found to be pH∼3.5) increases the redox potential for the pH-dependent redox processes, increasing the overpotential for the reduction of the species at the cathode.

The electrochemical studies are consistent with results from *operando* XANES measurements and the microbiological studies performed here. Namely, the high pH and high voltages observed in the anodic chamber near the glass wool interface favour the formation of highly oxidized iodine species, which we observe using XANES, and which are seen to rapidly inactivate *E. coli* at low current densities and short contact times. Further, electrochemical studies also confirm that pH and voltage in the cathodic chamber favours the reduction of oxidized species to iodide, which was the sole iodine product observed by XANES in the effluent.

While our studies demonstrate favourable conditions in the cathodic chambers for reduction of iodine species to iodide (along with XANES measurements that detect only iodide in the reactor effluent), the potential formation and/or accumulation of trace by-products that are below the detection limit of the techniques used in this work cannot be ruled out. The production of oxidation refractory intermediates including disinfection by-products is a limitation of many eAOPs, though a previous study screening for routine disinfection by-products has shown that effluent from the BioLargo AOS contains lower levels of known disinfection by-products than municipal tap water.[56]

As discussed at the outset of this paper, eAOPs are a promising class of treatment technologies to provide effective treatment of wastewater for reuse, but have several downsides, most notably high electricity consumption. This study demonstrates that the eAOP examined herein, the BioLargo AOS, is capable of achieving high rates of bacterial inactivation while using a lower current density and a shorter contact time than conventional eAOPs. This suggests that this eAOP may either itself serve as the basis for an effective and scalable wastewater treatment solution, or may be a useful component of a treatment train aimed at providing treatment for municipal or industrial wastewater. Furthermore, the characterization of the iodine-based eAOP described herein provides a basis for future work to improve other eAOPs for use in water treatment. While traditionally, eAOPs have suffered from poor energy consumption and therefore cost-efficiency, the significant improvement in current density required for bacterial inactivation observed with the AOS suggests there is potential for refinement of

eAOP reactors to maximize contaminant removal kinetics relative to input costs, stemming from the exploitation of previously unused halide species of higher oxidation potential.

ACKNOWLEDGMENTS

We thank Arlene Oatway at the Unversity of Alberta Department of Biological Sciences Microscopy Facility for assistance with electron microscopy. Part of the research described in this paper was performed at the Canadian Light Source, a national research facility of the University of Saskatchewan, which is supported by the Canada Foundation for Innovation (CFI), the Natural Sciences and Engineering Research Council (NSERC), the National Research Council (NRC), the Canadian Institutes of Health Research (CIHR), the Government of Saskatchewan, and the University of Saskatchewan. We thank the Natural Sciences and Engineering Research Council of Canada for support through NSERC Engage and Engage PLUS grants [KM: EGP-499182-16, EGP2-507089-17; ER: EGP-503902-16, EGP2-523101-18].

[Declaration of interest statement.] NB, RA, KM, ZF, and ER received research support from BioLargo Inc., who have a patent on the reactor (US patent 10,654,731 B2). AM, AE, SH, JB, PP, CZ, LPF, CL, RS, and KC are or were employed by BioLargo Inc. KRC is the Chief Science Officer at BioLargo Inc. and RS is the President and Chief Executive Officer of BioLargo Water Inc. MWG received financial compensation as a consultant for BioLargo Inc., and is a shareholder of BioLargo Inc. NC and PB have no competing interests.

CONTRIBUTIONS

AM designed the multi-chamber AOS reactor, contributed to the planning and execution of AOS work, synchotron experiments, and editing of the manuscript.

AE contributed to the design and execution of synchrotron experiments and disinfection experiments, performed electron microscopy, and co-wrote the manuscript with MWG.

SH designed disinfection experiments and microbiological assays, and contributed to the design and execution of synchrotron experiments.

JB contributed to synchrotron experiments, data analysis, and writing and editing the manuscript.

PP and CZ contributed to disinfection experiments, synchrotron experiments, and data analysis.

CG contributed to disinfection experiments and data analysis of synchrotron experiments.

CL contributed to data analysis of synchrotron experiments.

LPF designed and performed microbiological assays, analyzed microbiology results, and contributed to writing and editing of the manuscript.

RS created the initial design for the flow through AOS, was involved in design and execution of all AOS experiments, and contributed to synchrotron experiments and editing the manuscript.

KRC is the CSO for BioLargo and was the initial concept inventor and patent holder for the AOS, and was involved in all planning and long term research for the AOS.

All authors affiliated with BioLargo Water Inc. contributed to overall experimental analysis related to BioLargo AOS research.

NC and PERB contributed to synchrotron experiments.

NB contributed to synchrotron experiments, microbiological experiments, and editing the manuscript.

RA contributed to synchrotron experiments.

KM supervised NB, contributed to synchrotron experiments, and contributed to writing and editing the manuscript.

ZF designed and performed ex-situ voltammetry and operando potential distribution measurements, analyzed electrochemical data, and contributed to writing and editing the manuscript.

ER designed the setup for operando potential distribution measurements, supervised ZF for all electrochemical experiments and interpretation of the electrochemical data, and contributed to writing and editing the manuscript.

MWG conceived and designed synchrotron experiments, supervised synchrotron experiments, wrote the first draft of the manuscript, and co-wrote the manuscript with AE.

[1] F. C. Moreira, R. A. Boaventura, E. Brillas, and V. J. Vilar, "Electrochemical advanced oxidation processes: A review on their application to synthetic and real wastewaters," Appl. Catal. B Environ. **202**, 217–261 (2017).

[2] D. B. Miklos, C. Remy, M. Jekel, K. G. Linden, J. E. Drewes, and U. Hübner, "Evaluation of advanced oxidation processes for water and wastewater treatment – A critical review," Water Res. **139**, 118–131 (2018).

[3] S. O. Ganiyu, C. A. Martínez-Huitle, and M. A. Oturan, "Electrochemical advanced oxidation processes for wastewater treatment: Advances in formation and detection of reactive species and mechanisms," Curr. Opin. Electrochem. **27**, 100678 (2021).

[4] L. Feng, E. D. van Hullebusch, M. A. Rodrigo, G. Esposito, and M. A. Oturan, "Removal of residual anti-inflammatory and analgesic pharmaceuticals from aqueous systems by electrochemical advanced oxidation processes. A review," Chem. Eng. J. **228**, 944–964 (2013).

[5] C. A. Martínez-Huitle and S. Ferro, "Electrochemical oxidation of organic pollutants for the wastewater treatment: Direct and indirect processes," Chem. Soc. Rev. **35**, 1324–1340 (2006).

[6] P. Drogui, S. Elmaleh, M. Rumeau, C. Bernard, and A. Rambaud, "Hydrogen peroxide production by water electrolysis: Application to disinfection," J. Appl. Electrochem. **31**, 877–882 (2001).

[7] J. Jeong, C. Kim, and J. Yoon, "The effect of electrode material on the generation of oxidants and microbial inactivation in the electrochemical disinfection processes," Water Res. **43**, 895–901 (2009).

[8] L. H. Tran, P. Drogui, G. Mercier, and J. F. Blais, "Electrochemical degradation of polycyclic aromatic hydrocarbons in creosote solution using ruthenium oxide on titanium expanded mesh anode," J. Hazard. Mater. **164**, 1118–1129 (2009).

[9] E. Lacasa, E. Tsolaki, Z. Sbokou, M. A. Rodrigo, D. Mantzavinos, and E. Diamadopoulos, "Electrochemical disinfection of simulated ballast

water on conductive diamond electrodes," Chem. Eng. J. **223**, 516–523 (2013).

[10]R. Daghrir, P. Drogui, J. Tshibangu, N. Delegan, and M. A. El Khakani, "Electrochemical treatment of domestic wastewater using boron-doped diamond and nanostructured amorphous carbon electrodes," Environ. Sci. Pollut. Res. **21**, 6578–6589 (2014).

[11]S. Ghasemian, B. Asadishad, S. Omanovic, and N. Tufenkji, "Electrochemical disinfection of bacteria-laden water using antimony-doped tin-tungsten-oxide electrodes," Water Res. **126**, 299–307 (2017).

[12]C. A. Martínez-Huitle and M. Panizza, "Electrochemical oxidation of organic pollutants for wastewater treatment," Curr. Opin. Electrochem. **11**, 62–71 (2018).

[13]S. O. Ganiyu, M. Zhou, and C. A. Martínez-Huitle, "Heterogeneous electro-Fenton and photoelectro-Fenton processes: A critical review of fundamental principles and application for water/wastewater treatment," Appl. Catal. B Environ. **235**, 103–129 (2018).

[14]O. Ganzenko, C. Trellu, S. Papirio, N. Oturan, D. Huguenot, E. D. van Hullebusch, G. Esposito, and M. A. Oturan, "Bioelectro-Fenton: evaluation of a combined biological—advanced oxidation treatment for pharmaceutical wastewater," Environ. Sci. Pollut. Res. **25**, 20283–20292 (2018).

[15]O. Ganzenko, D. Huguenot, E. D. van Hullebusch, G. Esposito, and M. A. Oturan, "Electrochemical advanced oxidation and biological processes for wastewater treatment: A review of the combined approaches," Environ. Sci. Pollut. Res. **21**, 8493–8524 (2014).

[16]M. Mascia, A. Vacca, and S. Palmas, "Fixed bed reactors with three dimensional electrodes for electrochemical treatment of waters for disinfection," Chemical Engineering Journal **211-212**, 479–487 (2012).

[17]D. Ghernaout and B. Ghernaout, "From chemical disinfection to electrodisinfection: The obligatory itinerary?" Desalin. Water Treat. **16**, 156–175 (2010).

[18]D. Ghernaout, A. Badis, A. Kellil, and B. Ghernaout, "Application of electrocoagulation in Escherichia coli culture and two surface waters," Desalin. **219**, 118–125 (2008).

[19]M. Okochi, H. Yokokawa, T. K. Lim, T. Taguchi, H. Takahashi, H. Yokouchi, T. Kaiho, A. Sakuma, and T. Matsunaga, "Disinfection of microorganisms by use of electrochemically regenerated periodate," Appl. Environ. Microbiol. **71**, 6410–6413 (2005).

[20]M. Beppu, H. Ochiai, and K. Kikugawa, "Macrophage recognition of periodate-treated erythrocytes: Involvement of disulfide formation of the erythrocyte membrane proteins," BBA Biomembr. **979**, 35–45 (1989).

[21]K. P. Drees, M. Abbaszadegan, and R. M. Maier, "Comparative electrochemical inactivation of bacteria and bacteriophage," Water Res. **37**, 2291–2300 (2003).

[22]H. F. Diao, X. Y. Li, J. D. Gu, H. C. Shi, and Z. M. Xie, "Electron microscopic investigation of the bactericidal action of electrochemical disinfection in comparison with chlorination, ozonation and Fenton reaction," Process Biochem. **39**, 1421–1426 (2004).

[23]M. Mascia, A. Vacca, and S. Palmas, "Electrochemical treatment as a pre-oxidative step for algae removal using Chlorella vulgaris as a model organism and BDD anodes," Chem. Eng. J. **219**, 512–519 (2013).

[24]Y. Long, J. Ni, and Z. Wang, "Subcellular mechanism of Escherichia coli inactivation during electrochemical disinfection with boron-doped diamond anode: A comparative study of three electrolytes," Water Res. **84**, 198–206 (2015).

[25]X. Huang, Y. Qu, C. A. Cid, C. Finke, M. R. Hoffmann, K. Lim, and S. C. Jiang, "Electrochemical disinfection of toilet wastewater using wastewater electrolysis cell," Water Res. **92**, 164–172 (2016).

[26]C. E. Schaefer, C. Andaya, and A. Urtiaga, "Assessment of disinfection and by-product formation during electrochemical treatment of surface water using a ti/iro2 anode," Chem. Eng. J. **264**, 411–416 (2015).

[27]C. A. Martínez-Huitle and E. Brillas, "A critical review over the electrochemical disinfection of bacteria in synthetic and real wastewaters using a boron-doped diamond anode," Curr. Opin. Solid State Mater. Sci. **25**, 100926–100926 (2021).

[28]V. Schmalz, T. Dittmar, D. Haaken, and E. Worch, "Electrochemical disinfection of biologically treated wastewater from small treatment systems by using boron-doped diamond (BDD) electrodes - Contribution for direct reuse of domestic wastewater," Water Res. **43**, 5260–5266 (2009).

[29]S. Cotillas, J. Llanos, M. A. Rodrigo, and P. Cañizares, "Use of carbon felt cathodes for the electrochemical reclamation of urban treated wastewaters," Appl. Catal. B Environ. **162**, 252–259 (2015).

[30]P. V. Nidheesh, M. Zhou, and M. A. Oturan, "An overview on the removal of synthetic dyes from water by electrochemical advanced oxidation processes," Chemosphere **197**, 210–227 (2018).

[31]I. Sirés, E. Brillas, M. A. Oturan, M. A. Rodrigo, and M. Panizza, "Electrochemical advanced oxidation processes: Today and tomorrow. A review," Environ. Sci. Pollut. Res. **21**, 8336–8367 (2014).

[32]M. Cho, J. Kim, J. Y. Kim, J. Yoon, and J. H. Kim, "Mechanisms of Escherichia coli inactivation by several disinfectants," Water Res. **44**, 3410–3418 (2010).

[33]J. Jeong, J. Y. Kim, and J. Yoon, "The Role of Reactive Oxygen Species in the Electrochemical Inactivation of Microorganisms," Environ. Sci. Technol. **40**, 6117–6122 (2006).

[34]S. W. da Silva, J. B. Welter, L. L. Albornoz, A. N. A. Heberle, J. Z. Ferreira, and A. M. Bernardes, "Advanced Electrochemical Oxidation Processes in the Treatment of Pharmaceutical Containing Water and Wastewater: a Review," Curr. Pollut. Rep. **7**, 146–159 (2021).

[35]M. A. Oturan and J. J. Aaron, "Advanced oxidation processes in water/wastewater treatment: Principles and applications. A review," Crit. Rev. Environ. Sci. Technol. **44**, 2577–2641 (2014).

[36]C. Zhang, Y. Jiang, Y. Li, Z. Hu, L. Zhou, and M. Zhou, "Three-dimensional electrochemical process for wastewater treatment: A general review," Chem. Eng. J. **228**, 455–467 (2013).

[37]B. P. Chaplin, "The Prospect of Electrochemical Technologies Advancing Worldwide Water Treatment," Acc. Chem. Res. **52**, 596–604 (2019).

[38]F. C. Walsh and C. Ponce de León, "Progress in electrochemical flow reactors for laboratory and pilot scale processing," Electrochim. Acta **280**, 121–148 (2018).

[39]M. Sillanpää, M. C. Ncibi, and A. Matilainen, "Advanced oxidation processes for the removal of natural organic matter from drinking water sources: A comprehensive review," J. Environ. Manage. **208**, 56–76 (2018).

[40]B. C. Hodges, E. L. Cates, and J. H. Kim, "Challenges and prospects of advanced oxidation water treatment processes using catalytic nanomaterials," Nat. Nanotechnol. **13**, 642–650 (2018).

[41]R. Dewil, D. Mantzavinos, I. Poulios, and M. A. Rodrigo, "New perspectives for Advanced Oxidation Processes," J. Environ. Manage. **195**, 93–99 (2017).

[42]P. Cañizares, R. Paz, C. Sáez, and M. A. Rodrigo, "Costs of the electrochemical oxidation of wastewaters: A comparison with ozonation and Fenton oxidation processes," J. Environ. Manage. **90**, 410–420 (2009).

[43]T. J. Davies, M. E. Hyde, and R. G. Compton, "Nanotrench arrays reveal insight into graphite electrochemistry," Angew. Chem. Int. Ed. **44**, 5121–5126 (2005).

[44]M. Velický, P. S. Toth, C. R. Woods, K. S. Novoselov, and R. A. W. Dryfe, "Electrochemistry of the basal plane versus edge plane of graphite revisited," J. Phys. Chem. C **123**, 11677–11685 (2019).

[45]Y. Kong, J. Yuan, Z. Wang, S. Yao, and Z. Chen, "Application of expanded graphite/attapulgite composite materials as electrode for treatment of textile wastewater," Appl. Clay Sci. **46**, 358–362 (2009).

[46]M. Wissler, "Graphite and carbon powders for electrochemical applications," J. Power Sources **156**, 142–150 (2006).

[47]A. Evans, "BioLargo, Inc.: BioLargo spotlight: Update on the AOS poultry pilot," (2019).

[48]A. Evans, "BioLargo, Inc.: BioLargo completes manufacture of first commercial-scale AOS unit for municipal wastewater treatment plant," (2021).

[49]W. Gottardi, "Iodine as disinfectant," in *Iodine Chemistry and Applications*, edited by T. Kaiho (John Wiley & Sons Incorporated, 2014).

[50]W. Gottardi, "Iodine and disinfection: Theoretical study on mode of action, efficiency, stability, and analytical aspects in the aqueous system," Arch. Pharm. **332**, 151–157 (1999).

[51] G. Mcdonnell and A. D. Russell, "Antiseptics and disinfectants: Activity, action, and resistance," Clin. Microbiol. Rev. **12**, 147–179 (1999).

[52] D. T. Jiang, N. Chen, L. Zhang, K. Malgorzata, G. Wright, R. Igarashi, D. Beauregard, M. Kirkham, and M. McKibben, "XAFS at the Canadian Light Source," AIP Conf. Proc. **882**, 893–895 (2007).

[53] B. Ravel and M. Newville, "ATHENA, ARTEMIS, HEPHAESTUS : data analysis for X-ray absorption spectroscopy using IFEFFIT," J. Synchrotron Radiat. **12**, 537–541 (2005).

[54] A. M. A. Moustafa, K. N. McPhedran, J. Moreira, and M. Gamal El-Din, "Investigation of mono/competitive adsorption of environmentally relevant ionized weak acids on graphite: Impact of molecular properties and thermodynamics," Environ. Sci. Technol. **48**, 14472–14480 (2014).

[55] *Reregistration eligibility decision for iodine and iodophor complexes* (739-R-06-010, United States Environmental Protection Agency, 2006) p. 76.

[56] Y. He, L. Patterson-Fortin, J. Boutros, R. Smith, and G. G. Goss, "Removal of biological effects of organic pollutants in municipal wastewater by a novel advanced oxidation system," J. Environ. Manage. **280**, 111855 (2021).

[57] M. A. and Hayat and S. E. Miller, *Negative Staining* (McGraw-Hill, New York, 1990) p. 256.

[58] M. Berney, F. Hammes, F. Bosshard, H.-U. Weilenmann, and T. Egli, "Assessment and interpretation of bacterial viability by using the live/dead baclight kit in combination with flow cytometry," Appl. Environ. Microbiol. **73**, 3283–3290 (2007).

[59] S. Chen, W. Hu, J. Hong, and S. Sandoe, "Electrochemical disinfection of simulated ballast water on PbO2/graphite felt electrode," Mar. Pollut. Bull. **105**, 319–323 (2016).

[60] C. Heim, M. Ureña de Vivanco, M. Rajab, E. Müller, T. Letzel, and B. Helmreich, "Rapid inactivation of waterborne bacteria using boron-doped diamond electrodes," Int. J. Environ. Sci. Technol. **12**, 3061–3070 (2015).

[61] B. Schorr, H. Ghanem, S. Rosiwal, W. Geißdörfer, and A. Burkovski, "Elimination of bacterial contaminations by treatment of water with boron-doped diamond electrodes," World J. Microbiol. Biotechnol. **35**, 48 (2019).

[62] Z. Frontistis, C. Brebou, D. Venieri, D. Mantzavinos, and A. Katsaounis, "BDD anodic oxidation as tertiary wastewater treatment for the removal of emerging micro-pollutants, pathogens and organic matter," J. Chem. Technol. Biotechnol. **86**, 1233–1236 (2011).

[63] W. A. Reed, I. May, F. R. Livens, J. M. Charnock, A. P. Jeapes, M. Gresley, R. M. Mitchell, and P. Knight, "Xanes fingerprinting of iodine species in solution and speciation of iodine in spent solvent from nuclear fuel reprocessing," J. Anal. At. Spectrom. **17**, 541–543 (2002).

[64] Y. S. Shimamoto, T. Itai, and Y. Takahashi, "Soil column experiments for iodate and iodide using k-edge xanes and hplc-icp-ms," J. Geochem. Explor. **107**, 117–123 (2010).

[65] N. Yamaguchi, M. Nakano, R. Takamatsu, and H. Tanida, "Inorganic iodine incorporation into soil organic matter: evidence from iodine k-edge x-ray absorption near-edge structure," J. Environ. Radioact. **101**, 451–457 (2010).

[66] C. Verwold, A. Ortega-Hernandez, J. Murakami, L. Patterson-Fortin, J. Boutros, R. Smith, and S. Y. Kimura, "New iodine-based electrochemical advanced oxidation system for water disinfection: Are disinfection by-products a concern?" Water Res. **201**, 117340 (2021).

[67] A. J. Bard and L. R. Faulkner, *Electrochemical methods: fundamentals and applications*, 2nd ed. (Wiley, New York, 2000).

[68] R. H. Wopschall and I. Shain, "Effects of Adsorption of Electroactive Species in Stationary Electrode Polarography," Anal. Chem. **39**, 1514–1527 (1967).

[69] R. H. Wopschall and I. Shain, "Adsorption Characteristics of the Methylene Blue System Using Stationary Electrode Polarography," Anal. Chem. **39**, 1527–1534 (1967).

[70] R. S. Kumar, S. Sornambikai, N. S. Karthikeyan, K. Sathiyanarayanan, and A. Senthil, "A Simple Colorimetric Screening of Nitrite Using Iodide in an Acidic pH Solution," Austin J. Anal. Pharm. Chem. **1**, 1–3 (2014).

[71] G. Dryhurst and P. J. Elving, "Electrooxidation of Halides at Pyrolytic Graphite Electrode in Aqueous and Acetonitrile Solutions," Anal. Chem. **39**, 606–615 (1967).

[72] E. Cho, A. Perebikovsky, O. Benice, S. Holmberg, M. Madou, and M. Ghazinejad, "Rapid iodine sensing on mechanically treated carbon nanofibers," Sensors **18**, 1486 (9pp)–1486 (9pp) (2018).

[73] L. M. Dané, L. J. J. Janssen, and J. G. Hoogland, "The iodine/iodide redox couple at a platinum electrode," Electrochim. Acta **13**, 507–518 (1968).

[74] A. Bard, R. Parson, and J. Jordon, *Standard potentials in aqueous solutions* (M. Dekker, New York, 1985).

[75] M. Torimura, K. Kano, T. Ikeda, M. Goto, and T. Ueda, "On-line electrochemical detection of carbohydrates coupled with the periodate oxidation," J. Chromatogr. A **790**, 1–8 (1997).

[76] T. Doherty, J. Sunderland, E. Roberts, and D. Pickett, "An improved model of potential and current distribution within a flow-through porous electrode," Electrochim. Acta **41**, 519–526 (1996).

For Table of Contents Only